Estimation of Maximum Displacement Response for Inelastic Oscillator based on Natural Period Dependent Spectrum Intensity

T. Furukawa[1] and Y. Mori[2]

[1] KAJIMA Technical Research Institute, Former Grad. Student, Nagoya University, Tokyo, Japan, furukata@kajima.com
[2] Professor, Nagoya University, Nagoya, Japan, yasu@nuac.nagoya-u.ac.jp

Abstract: In this study, a simplified method for estimating the maximum displacement of oscillators with bi-linear, bi-linear-slip, or tri-linear hysteresis curves is proposed. The method is based on a newly discovered simple relationship with the natural period dependent spectrum intensity, which is defined herein as an integration of an elastic acceleration response spectrum from the elastic natural period of the oscillator to the elongated natural period. The accuracy of the proposed method is investigated based on numerical examples. The results indicate that the bias of the estimates by the proposed method is significantly smaller than that of other methods, regardless of the types and characteristics of the oscillator. Additionally, the dispersion of the estimates by the proposed method is mostly smaller than that of the other methods. Moreover, the dispersion models of the proposed method are presented in this paper.

Keywords: inelastic response, oscillator, earthquake ground motion intensity, spectrum intensity.

1. General

For reliability-based seismic performance assessment and design of structures, the structural demand needs to be evaluated in a probabilistic sense. Such information for given structures can be obtained via a simulation-based approach (e.g., Collins et al. 1996) with nonlinear dynamic analysis (NDA). However, the seismic demand must be estimated for numerous earthquake records, which requires intensive computational effort. Thus, a predictor of seismic structural demands that is more time-efficient than NDA can be practically useful.

The calculation of response and limit strength method was introduced in the Japanese Building Code in 2000 as a seismic design rule for ordinary building structures. The predictor of structural demands in this method evaluates inter-story drifts, only considering the inelastic first-modal response. Luco and Cornell (2007) proposed a predictor, originally as an earthquake ground motion intensity measure (IM), that uses the square-root-of-sum-of-squares (SRSS) rule of modal combination and considers the first-mode inelastic spectral displacement. Mori et al. (2004, 2006) proposed a predictor based on Luco and Cornell's method that considers a post-elastic deflected shape for the first modal vector.

These techniques use the maximum displacement response of the inelastic oscillator, d_{max}, that is equivalent to the original frame. The IM, such as peak ground acceleration (PGA), peak ground velocity (PGV), and spectrum intensity (SI) (Housner 1952) have been used to predict d_{max}; whereas numerous studies on IM have shown that the appropriate IM for predicting the response of structures depend on the natural period, T_1, of the given structure. Although the elastic spectral response is a function of T_1, it does not consider the effect of the inelastic behavior of oscillators, which questions the accuracy and applicability of the d_{max} estimation method based on the elastic spectral response.

With respect to the aforementioned problem, Kitahara and Itoh (1999, 2000) proposed a new IM known as natural period dependent SI (noted as $SI_{n.p.}$ hereafter) that is applicable to bridge piers with a wide range of the natural period, and the d_{max} estimation method based on $SI_{n.p.}$. This IM is defined as an integration of an elastic velocity response spectrum, S_v; not from 0.1 s to 2.5 s as defined by Housner, but from $e \cdot T_1$ to $f \cdot T_1$ (e, f: constant values). Furthermore, Kadas et al. (2011) have proposed a modified $SI_{n.p.}$ for reinforced concrete (RC) frames. This is defined as an integration of an elastic acceleration response spectrum, S_a, between T_1 and the natural period elongated by the inelastic behavior of the oscillator equivalent to the RC frame, T_{el}, that is estimated for a given ground motion on the basis of the elastic acceleration spectral response. They demonstrated that the modified $SI_{n.p.}$ correlates better with the inelastic response of RC frames compared to other spectral intensities.

Optimally estimating d_{max} based on the general relationship between d_{max} and modified $SI_{n.p.}$ is important; however, Kadas et al. have not yet determined this relationship. In this study, it is found that the relationship between d_{max} and modified $SI_{n.p.}$ can be modeled by a simple linear function based on the NDA results of the oscillators with bi-linear, bi-linear-slip, or tri-linear hysteresis curves. Modified $SI_{n.p.}$ used in this study is defined as an integration of S_a from T_1 to T_{el} estimated by the maximum ductility factor, μ, of the oscillator, which is followed by the proposed d_{max} estimation method based on the combination of the above relationships and the elastic response spectrum of a given ground motion. Further, the accuracy of the proposed method is investigated using the NDA results.

2. Past Studies on Natural Period Dependent SI

Kitahara and Itoh proposed $SI_{n.p.}$ defined by the following equation for bridge piers. They showed that the correlation coefficient between $SI_{n.p.}$ and d_{max} of the oscillators equivalent to piers was 0.90-0.95, whereas the correlation coefficient between $PGVs$ and d_{max} was approximately 0.70-0.90.

$$SI_{n.p.} = \frac{1}{(f-e) \cdot T_1} \int_{e \cdot T_1}^{f \cdot T_1} S_v(T; h_1 = 0.05) dT \quad (1)$$

Here, h_1 is a damping factor of piers, e and f, which are set to 0.9 and 1.2, respectively, for steel piers and 1.0 and

2.8, respectively, for RC piers.

Kadas et al. proposed a modified $SI_{n.p.}$ defined by the following equation and showed the correlation coefficient between the modified $SI_{n.p.}$ and maximum inter-story drift ratio of RC frames was 0.792-0.992:

$$\text{modified } SI_{n.p.} = \int_{T_1}^{T_{el}} \frac{S_a(T; h_1 = 0.05)}{C_y \cdot g} \cdot \frac{T - T_1}{T_{el} - T_1} dT \quad (2)$$

where C_y is the yield base shear force coefficient of an oscillator equivalent to the RC frame and g is the gravitational acceleration. In addition, T_{el} is estimated by the following equation, which is obtained by modeling the relationship between the elastic acceleration spectral responses and the natural periods estimated based on the secant stiffness at the maximum response of the oscillator calculated via NDA:

$$T_{el} = 1.07 \cdot T_1 \cdot \{S_a(T; h_1 = 0.05)/(C_y \cdot g)\}^{0.45} \quad (3)$$

3. New Natural Period Dependent SI

This study defines a natural period dependent SI, SI_μ, as follows:

$$SI_\mu = \int_{T_1}^{T_{el}} S_a(T; h_1) dT \quad (4)$$

where T_{el} is the natural period elongated by the inelastic behavior of the oscillator. It is estimated with μ of the oscillators with bi-linear, bi-linear-slip, or tri-linear hysteresis curves as follows:

$$T_{el} = \begin{cases} [\text{Bi-liear, Bi-liear-slip}] \\ T_1 \sqrt{\dfrac{\mu}{1 - \alpha + \alpha \cdot \mu}} \\ [\text{Tri-liear}] \\ T_1 \sqrt{\dfrac{\mu}{1 - \alpha + \alpha \cdot \mu}} \quad (\mu < \mu_g) \\ T_g \sqrt{\dfrac{\mu/\mu_g}{1 - \alpha_g + \alpha_g \cdot \mu/\mu_g}} \quad (\mu \geq \mu_g) \end{cases} \quad (5)$$

Figure 1 presents the relationship between the shear force, Q, and displacement, d, of the oscillators with (a) bi-linear, bi-linear-slip, and (b) tri-linear hysteresis curve. Here, m is the mass, d_y and d_{y2} are the first and second yield displacements, respectively, $\mu_g = d_{y2}/d_y$, k is the elastic stiffness, k_g is the secant stiffness connecting origin and second break point, C_{y2} is the shear force coefficient at the second break point, T_g is the natural period according to k_g, α and $\alpha\beta$ are the ratios of the second and third slope, respectively, and $\alpha_g = \alpha\beta k/k_g$.
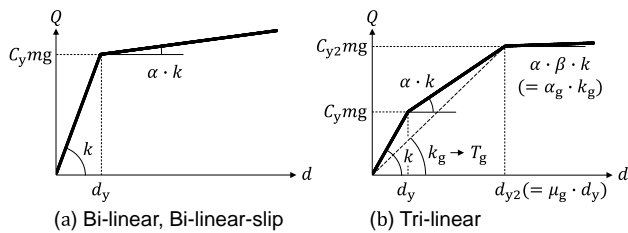

(a) Bi-linear, Bi-linear-slip   (b) Tri-linear

Figure 1 Parameters of hysteresis curve

4. Relationship between SI_μ and d_{max}

In this section, the general relationship between SI_μ and d_{max} is modeled based on the NDA results.

4.1 Ground motion records and inelastic oscillators

Considering the effect of the characteristics of various ground motions, this study uses 219 observed ground motions recorded mostly in the United States and Japan and 1400 simulated ground motions.

Of the 219 observed ground motions, (Furukawa et al., 2017) 108 were intraplate earthquakes of moment magnitude M=6.0-7.7, and the other 111 were interplate earthquakes (M=7.1-8.0), including 91 recorded during the Tohoku Region Pacific Coast earthquake that occurred on March 11, 2011 (Knet).

The simulated ground motions (Mori et al., 2018) consist of 6 sets of 50 ground motions, which consider different types of earthquakes such as interplate or intraplate, as well as soil conditions such as hard, medium, or soft. The ground motions in each set were normalized such that their PGVs equaled 0.5, 1.0, 1.5, or 2.0×10^3 (mm/s). The durations of the ground motions were set to 40.96 (s) and 163.84 (s) for intraplate and interplate earthquakes, respectively.

The oscillators with the following characteristics were considered:

[Bi-linear, Bi-linear-slip]
- T_1 =0.10, 0.15, 0.20, 0.25, 0.35, 0.5,0 0.75, 1.00, 1.25, 1.50, or 2.00 (s)
- C_y =0.20, 0.30, 0.40, 0.50, 0.60, or 0.70
- α =0.00, 0.03, 0.06, 0.10, 0.20, 0.30, 0.40, 0.50, 0.60, 0.70, 0.80, 0.90, or 0.99
- h_1 =0.02

[Tri-linear]
- T_1, α, h_1: Same values as bi-linear and bi-linear-slip
- C_y =0.20, 0.30, 0.40, or 0.50
- $C_{y2} = C_y + C_x$ where C_x =0.05, 0.10, 0.20, or 0.30
- $\alpha\beta$ where β =0.03, 0.06, 0.10, 0.20, 0.30, 0.40, 0.50, 0.60, 0.70, 0.80, 0.90, or 0.99

4.2 Analysis of relationship between SI_μ and d_{max}

The relationship between SI_μ and d_{max} is modeled using half of the ground motion records described in Section 4.1, and the other records are used to investigate the accuracy of the proposed method in Section 6. These records were divided such that they did not have a bias of characteristics for the ground motions.

Figure 2(a) presents the relationship between SI_μ and d_{max} of the oscillators with the bi-linear hysteresis curve ($T_1 = 0.50$, $\alpha = 0.00$ and $C_y = 0.20$, 0.40, and 0.60) calculated via NDA using the ground motions described above in the forms of $\ln(SI_\mu)$ and $\ln(d_y(\mu - 1))$. Notably, only the results within the range of $1 < \mu < 20$, which are generally of concern in structural engineering, were plotted in the figure. Because all the results are plotted closely along a single linear line, regardless of the C_y values, the relationship can be modeled by a linear function. As shown in Figure 2(a), the regression lines are also presented by a solid line as well as the dispersion of $\ln(d_y(\mu - 1))$ on $\ln(SI_\mu)$, σ_{SI}.
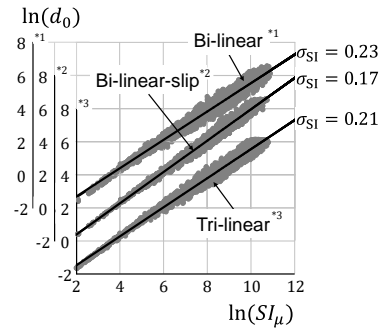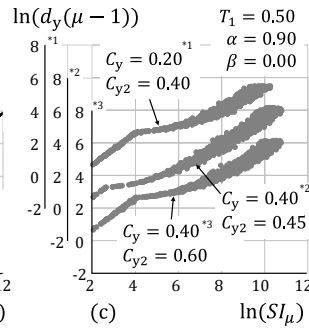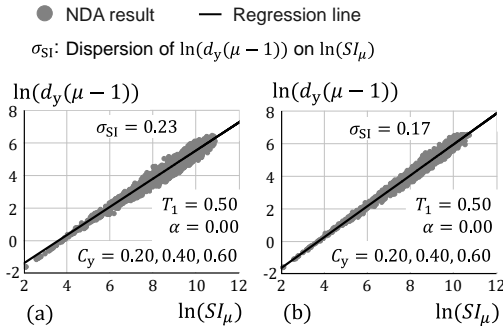
Figure 2 Relationship between $\ln(SI_\mu)$ and $\ln(d_y(\mu - 1))$ of the oscillator with (a) bi-linear, (b) bi-linear-slip, (c) tri-linear hysteresis curve $(1 < \mu < 20)$

Figure 3 Relationship between $\ln(SI_\mu)$ and $\ln(d_0)$ of the oscillator with each hysteresis curve

Figures 2(b) and (c) present the relationship between $\ln(SI_\mu)$ and $\ln(d_y(\mu - 1))$ for the oscillators with bi-linear-slip ($T_1 = 0.50$, $\alpha = 0.00$ and $C_y = 0.20$, 0.40, 0.60) and tri-linear ($T_1 = 0.50$, $\alpha = 0.90$, $\beta = 0.00$, $C_y = 0.20$, 0.40 and $C_{y2} = 0.40$, 0.45, 0.60) hysteresis curves, respectively. Additionally, the relationship in Figure 2(b) can be modeled by a linear function as the relationship in Figure 2(a); however, the relationship in Figure 2(c) cannot be modeled this way. Although not shown in Figure 2(c), the tendency of the relationship changed when the value of the vertical axis was equal to $\ln(d_y(\mu_g - 1))$ for all three oscillators with tri-linear hysteresis curves. Considering these observations, all of the results plotted in Figure 2 were re-plotted in Figure 3 with new vertical axes, $\ln(d_0)$, defined by the following equation, where all of the results were plotted closely to a single linear line for each hysteresis curve. d_0 is expressed in Figure 1 as the interception of $Q = 0$ and the linear line with the slope equal to k though the maximum response point.

$$d_0 = \begin{cases} \text{[Bi-liear, Bi-liear-slip]} \\ d_y(\mu - 1)(1 - \alpha) \\ \text{[Tri-liear]} \\ \begin{cases} d_y(\mu - 1)(1 - \alpha) & (\mu < \mu_g) \\ d_y(\mu - 1)(1 - \alpha) + d_g & (\mu \geq \mu_g) \end{cases} \end{cases} \quad (6)$$

where $d_g = d_y(\mu - \mu_g)(\alpha - \alpha\beta)$.

As shown in Figure 3, the results of the oscillators with the bi-linear and bi-linear-slip hysteresis curve in Figures 2(a) and (b) are moved in the upper direction by adding the constant value, $\ln(1 - \alpha)$, to the value of the vertical coordinate. In Figure 3, the result of the oscillators with the tri-linear hysteresis curve in Figure 2(c) are moved as well, and re-plotted on the new vertical axis, $\ln(d_y(\mu - 1)(1 - \alpha) + d_g)$, in the range of $\mu \geq \mu_g$.

4.3 Modeling relationship between SI_μ and $d_{\max}$
Results similar to Figure 3 were obtained for all the oscillators described in Section 4.1, and the relationship between $\ln(SI_\mu)$ and $\ln(d_0)$ is modeled by the linear function expressed by Eq. (7). The slope, A_1, and intercept, A_2, are estimated by Eqs. (8) and (9), respectively.

$$\ln(d_0) = A_1 \cdot \ln(SI_\mu) + A_2 \quad (7)$$

$$A_1 = B_1 \cdot \ln(T_1) + B_2/(T_1) + B_3 \quad (8)$$

$$A_2 = B_4 \cdot \ln(T_1) + B_5 \quad (9)$$

Here, B_p ($p = 1,2,3,4,5$) is estimated by substituting the values in Table 1 into Eq. (10).

$$B_p = \begin{cases} \text{[Bi-liear]} \\ b_{p,1}\alpha^3 + b_{p,2}\alpha^2 + b_{p,3}\alpha + b_{p,4}\sqrt{\alpha} + b_{p,5} \\ \text{[Bi-liear-slip]} \\ s_{p,1}\alpha^3 + s_{p,2}\alpha^2 + s_{p,3}\alpha + s_{p,4}\sqrt{\alpha} + s_{p,5} \\ \text{[Tri-liear]} \\ {}_1t_p\alpha^3 + {}_2t_p\alpha^2 + {}_3t_p\alpha + {}_4t_p\sqrt{\alpha} + {}_5t_p \end{cases} \quad (10)$$

where ${}_rt_p = {}_rt_{p,1}\beta^3 + {}_rt_{p,2}\beta^2 + {}_rt_{p,3}\beta + {}_rt_{p,4}\sqrt{\beta} + {}_rt_{p,5}$.

5. Proposed Estimation Method for $d_{\max}$
The value of $d_{\max}$ can be estimated as the intersection of the straight line modelled by Eq. (7), as well as the relationship between SI_μ (Eq. (4)) and d_0 (Eq. (6)) estimated by gradually increasing μ, and accordingly T_{el} (Eq. (5)) from T_1 for each ground motion. Hereafter, this relationship is referred to as the "spectrum line." Figure 4 presents the straight line modelled by Eq. (7) (solid line) and a spectrum line (dashed line) as well as the NDA result of an oscillator to a given ground motion (outlined circle). By definition, the NDA result is always located on the spectrum line of a given ground motion. Therefore, as shown in Figure 3, when the relationship has no dispersion, i.e. $\sigma_{SI} = 0$, μ of the estimate for the ground motion records is equal to μ calculated via NDA.
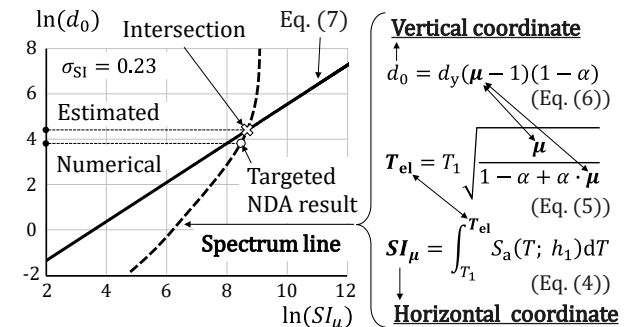

Figure 4 Proposed estimation method for $d_{\max}$

6. Accuracy of Proposed Method

6.1 Bias and dispersion
The accuracy of various estimation methods is expressed by its bias, a, defined by the median (or geometric mean) of μ of the estimate divided by μ calculated via NDA for

Table 1 $b_{p,q}$, $s_{p,q}$ and $_r t_{p,q}$ in Eqs. (10)

p	q	$b_{p,q}$	$s_{p,q}$	$_1t_{p,q}$	$_2t_{p,q}$	$_3t_{p,q}$	$_4t_{p,q}$	$_5t_{p,q}$
Slope, A_1 (Eq.(8))								
1	1	-0.1260	-0.1050	0.1690	-0.5970	0.4470	-0.1020	0
	2	0.2860	0.2480	-0.4280	1.2350	-0.7750	0.1590	0
	3	-0.1700	-0.1230	-0.1790	0.0830	-0.0990	0.0270	0
	4	0.0180	0	0.1960	-0.2340	0.1090	-0.0250	0
	5	-0.0020	-0.0170	0.0080	-0.0050	0.0200	-0.0040	-0.0016
2	1	0	0.0030	-0.0450	-0.0700	0.1590	-0.0440	0
	2	0.0260	0	-0.0030	0.2790	-0.3440	0.0860	0
	3	-0.0570	-0.0220	0.0960	-0.2960	0.1880	-0.0310	0
	4	0.0270	0.0150	-0.0353	0.0708	-0.0144	-0.0016	0
	5	0.0060	0.0050	-0.0147	0.0439	-0.0462	0.0185	0.0061
3	1	0	-0.0310	0	0	0	0	0
	2	-0.0280	0	-0.1230	0.1140	0.0440	0.0010	0
	3	0.2800	0.1000	-0.1870	0.2700	0.0250	-0.0300	0
	4	-0.1130	0	0.0730	-0.0720	-0.0570	0.0220	0
	5	0.8580	0.9280	0.2820	-0.4530	0.3480	-0.1200	0.8580
Intercept, A_2 (Eq.(9))								
4	1	0	0.55	0	0	0	0	0
	2	0.09	-0.97	0	0	0	0	0
	3	-0.72	0.08	3.35	-5.00	1.71	-0.18	0
	4	0.43	0.15	-1.90	2.32	-0.35	-0.02	0
	5	1.19	1.19	-0.52	1.02	-0.84	0.22	1.19
5	1	0	0	0	0	0	0	0
	2	0.32	0.30	2.17	-2.73	0.50	-0.13	0
	3	-1.54	-0.53	0	0	0	0	0
	4	0.56	-0.05	0	0	0	0	0
	5	-2.34	-2.70	-1.95	2.76	-1.78	0.51	-2.34
Dispersion, $\hat{\sigma}$ (Eq.(13))								
6	1	-0.800	0.060	-0.460	0.380	0.080	0	0
	2	1.340	0	0	0	0	0	0
	3	-0.430	0.040	-0.300	0.720	-0.280	0	0
	4	0	0	0	0	0	0	0
	5	-0.130	-0.110	-0.730	1.230	-0.530	0	-0.140
7	1	-0.390	0.060	-0.166	0.263	-0.035	0	0
	2	0.810	0	0	0	0	0	0
	3	-0.530	-0.070	-0.077	0.194	-0.166	0	0
	4	0.090	0	0	0	0	0	0
	5	0.020	0.017	-0.135	0.266	-0.152	0	0.015
8	1	0	-0.110	-0.070	-0.080	0.040	0	0
	2	-0.270	0	0	0	0	0	0
	3	0	-0.110	0.180	-0.500	0.110	0	0
	4	0	0	0	0	0	0	0
	5	0.280	0.240	0.260	-0.330	0.090	0	0.300

the j th ground motion records, $\mu_{\text{est},j}/\mu_{\text{NDA},j}$, and its dispersion, σ, defined by the standard deviation of the natural logarithms of $\mu_{\text{est},j}/\mu_{\text{NDA},j}$ is estimated by the following equations. The bias and dispersion are equivalently obtained by performing a one-parameter log-log linear least-squares regression of $\mu_{\text{NDA},j}$ on $\mu_{\text{est},j}$.

$$a = \exp\left\{\frac{1}{n}\sum_{j=1}^{n}\ln(\mu_{\text{NDA},j}) - \frac{1}{n}\sum_{j=1}^{n}\ln(\mu_{\text{est},j})\right\} \tag{11}$$

$$\sigma = \sqrt{\frac{1}{n-2}\sum_{j=1}^{n}\left[\ln(\mu_{\text{NDA},j}) - \{\ln(a) + \ln(\mu_{\text{est},j})\}\right]^2} \tag{12}$$

6.2 Results

Figures 5 presents the comparison between μ_{NDA} and μ_{est} in the log-log scale for the oscillators with the bi-linear hysteresis curve ($T_1 =$ (1) 0.20, (2) 0.50, (3) 1.50 and $\alpha =$ (a) 0.00, (b) 0.10, (c) 0.90) subjected to the ground motions not used in Sections 4.2, 4.3. The results of all oscillators with different C_y values are presented together in each part of Figure 5, as similar results were obtained regardless of C_y, given a combination of T_1 and α. In each figure, the regression line with a slope equal to unity and the one-to-one straight line are presented by a solid line and a dotted line, respectively, along with a, σ, and σ_{SI} values.

For all the oscillators shown in Figure 5, a was relatively close to unity. On the contrary, σ became large when T_1 was short and α was small. The following two factors could increase σ: the effect of σ_{SI} as described in Section 5 as well as the difference between the slope of the straight line modelled by Eq. (7) and that of the spectrum lines. As shown in Figure 5, σ_{SI} for the oscillators with T_1= 0.20 and α= 0.00 was not significantly larger than σ_{SI} for the other oscillators. On the contrary, although not presented in this paper, the slopes of the straight line modelled by Eq. (7) was similar to those of several spectrum lines when T_1 was short and α was small (Furukawa and Mori, 2020).

The accuracy of the proposed method was investigated by comparing the energy conservation rule, displacement conservation rule, equivalent linearization technique (ELT), and the estimation method using $SI_{\text{n.p.}}$ with an integration range from $1.0 \cdot T_1$ to $2.8 \cdot T_1$ (noted as $SI_{\text{n.p.}}$ method hereafter). Among the ELTs proposed previously, the equivalent natural period estimated by Eq. (5) and the damping reduction factor for the response spectra proposed by Kasai (2003) were used in this study. Furthermore, this study utilized the equivalent damping factor proposed by Shimazaki (1999) for the oscillators with the bi-linear hysteresis curve and the factor estimated with the hysteretic energy dissipation and maximum strain energy (Jennings, 1963) for the oscillators with the bi-linear-slip and tri-linear hysteresis curve.

Figure 6 presents the comparison between μ_{NDA} and μ_{est} estimated by previous methods for the oscillators with the bi-linear hysteresis curve (T_1= 0.20 and α= 0.00). The bias, a, of the proposed method was closer to unity, and the dispersion, σ, was smaller than those of the other four methods (Figure 5 (a-1)).
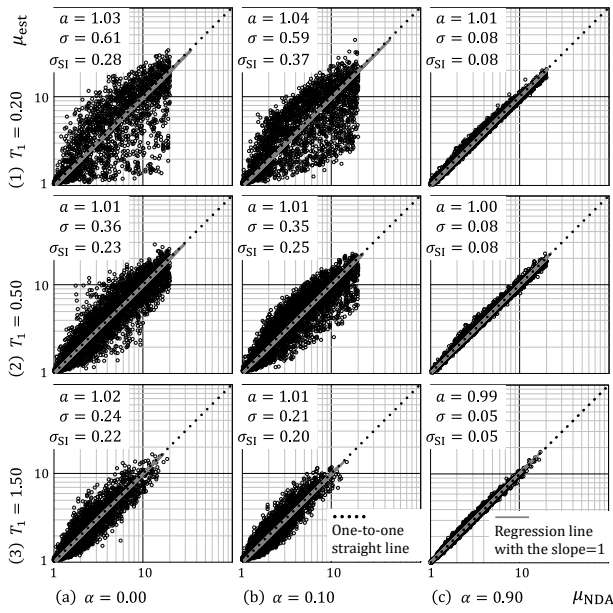
Figure 5 Comparison between μ_{NDA} and μ_{est} estimated by the proposed method (Bi-linear, $1 < \mu_{\text{NDA}} < 20$)

Figure 6 Comparison between μ_{NDA} and μ_{est} estimated by the previous methods (Bi-linear, $T_1 = 0.20$ and $\alpha = 0.00$)

Figure 7 presents a and σ of the estimators (a) as a function of T_1 of the oscillators with a bi-linear hysteresis curve of $\alpha = 0.00$, and (b) as a function of α of the oscillators with $T_1 = 0.50$. Moreover, this figure depicts a and σ by an outlined circle obtained using the straight lines of the slopes and intercepts that were not estimated by Eqs. (8) and (9), rather calculated directly by the regression analysis. The dashed line in the lower part of Figure 7 indicates the dispersions of the proposed method, $\hat{\sigma}$, modelled by the following:

$$\hat{\sigma} = B_6 \cdot \ln(T_1) + B_7/(T_1) + B_8 \qquad (13)$$

Here, B_p ($p = 6, 7, 8$) is estimated by substituting the values in Table 1 into Eq. (10).

As shown in Figure 7, a of the proposed method was approximately equal to unity for all of the oscillators. In addition, σ of the method was smaller than or approximately equal to those of the previous methods. Both of the results, the outlined circle and $\hat{\sigma}$, were approximately equal to those of the proposed method.

Figure 8 presents a and σ for the oscillators with a bi-linear-slip hysteresis curve. Figure 9 presents a and σ for the oscillators with a tri-linear hysteresis curve as a function of T_1 of the oscillators with (a) $\alpha = 0.10$, $\beta = 0.00$, (b) $\alpha = 0.10$, $\beta = 0.90$, and as a function of α of the oscillators with (c) $T_1 = 0.50$, $\beta = 0.00$, (d) $T_1 = 0.50$, $\beta = 0.90$. As the results in the Figure 7, the results in Figure 8 and 9 indicated that a of the proposed method is close to unity and σ of the proposed method is approximately smaller than those of the previous methods.

7. Conclusions

In this study, it was observed that the relationship between the maximum displacement response of the oscillators with bi-linear, bi-linear-slip, or tri-linear hysteresis curves and the natural period dependent spectrum intensity, SI_μ, can be modeled using a simple linear function. SI_μ is defined
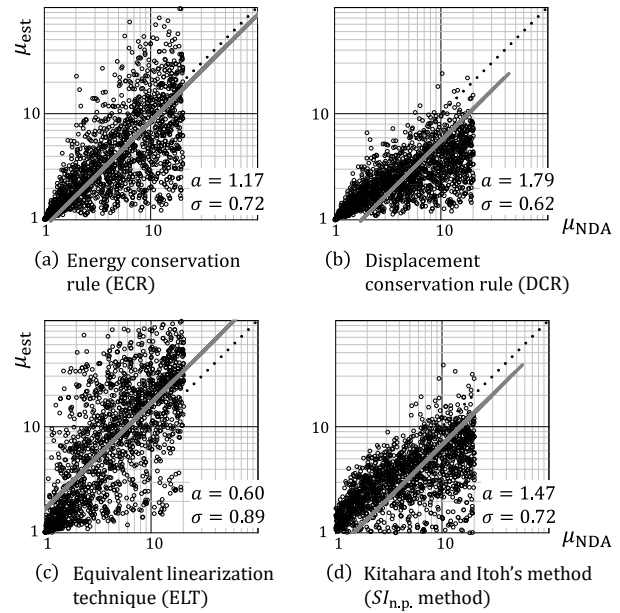
as an integration of an elastic acceleration response spectrum from the elastic natural period of the oscillator to the elongated natural period, estimated by the maximum ductility factor of the oscillator. Subsequently, a maximum displacement response of the oscillator based on the combination of the linear relationships and elastic response spectrum of a given ground motion was proposed.

The bias of the estimates by the proposed method is fairly close to unity, and the dispersion of the estimates using the proposed method was mostly smaller than those of the energy or displacement conservation rule, the equivalent linearization technique and the estimation method using a past natural period-dependent spectrum intensity. In addition, the dispersion of the proposed method can be estimated by Eq. (13).

Further investigations considering general hysteresis curves will be conducted to improve the applicability and versatility of the proposed method. Moreover, the seismic hazard at a site expressed in terms of SI_μ will be studied for reliability-base limit state design.

8. Acknowledgments

References

Collins, K. R., Wen, Y. K., and Foutch, D. A. 1996. Dual-level seismic design: a reliability-based methodology. *Earthquake Engineering and Structural Dynamics*, Vol. 25, pp. 1433-1467.

Furukawa, T., Kang, J. D., and Mori, Y. 2017. Simplified method for estimating maximum drift of multi-story steel frame with hysteretic dampers. *Journal of Structural and Construction Engineering* (*Transactions of AIJ*), Vol. 82, No. 740, pp. 1589-1599. (in Japanese)
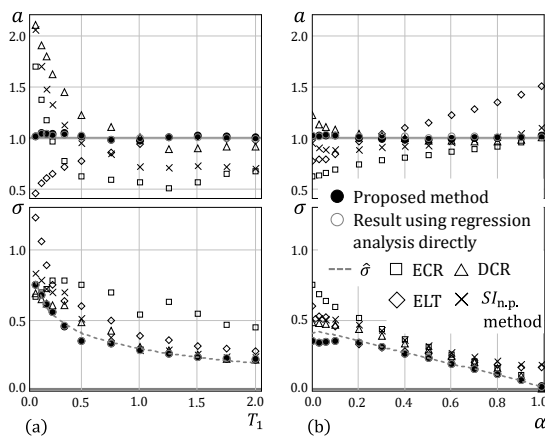
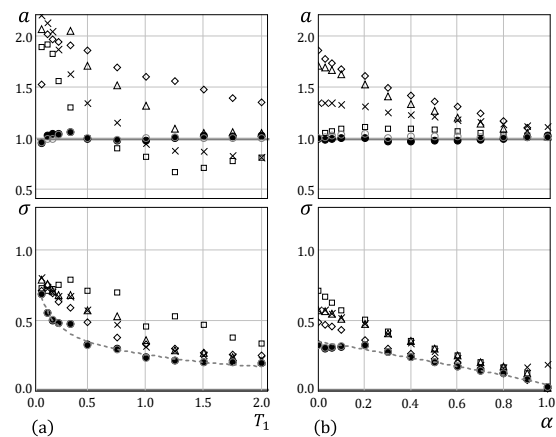Figure 7 a and σ (Bi-linear, (a) $\alpha = 0.00$, (b) $T_1 = 0.50$)

Figure 8 a and σ (Bi-linear-slip, (a) $\alpha = 0.00$, (b) $T_1 = 0.50$)

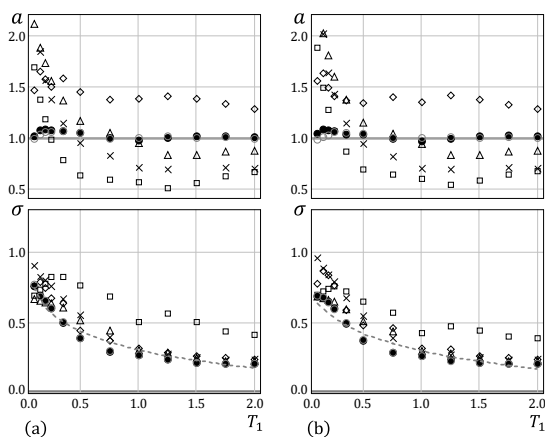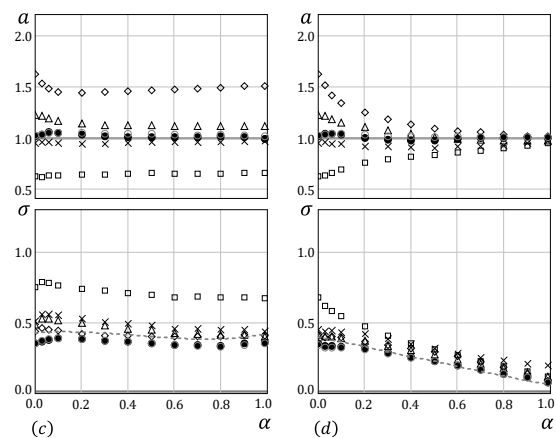Figure 9 a and σ (Tri-linear, (a) $\alpha = 0.10$, $\beta = 0.00$, (b) $\alpha = 0.10$, $\beta = 0.90$, (c) $T_1 = 0.50$, $\beta = 0.00$, (d) $T_1 = 0.50$, $\beta = 0.90$)

Furukawa, T. and Mori, Y. 2020. Simplified method for estimating maximum displacement of inelastic oscillator based on natural period-dependent spectrum intensity. *Journal of Structural and Construction Engineering (Transactions of AIJ)*, Vol. 85, No. 773. (accept) (in Japanese)

Jennings, P. C. 1963. Equivalent Viscous Damping for Yielding Structures. *Journal of Structural Engineering*, ASCE, Vol. 35, No. 11, pp. 1706-1711.

Housner, G. W. 1952. Spectrum intensity of storing motion earthquakes. *Proceedings of Symposium on Earthquake and Blast Effects on Structures,* pp. 20-36.

K-NET, <http://www.kyoshin.bosai.go.jp>, accessed October 1st, 2017.

Kadas, K., Yakut, A., and Kazaz, I. 2011. Spectral ground motion intensity based on capacity and period elongation. *Journal of Structural Engineering*, ASCE, Vol. 137, No. 2, pp. 401-409.

Kasai, K., Ito, H., and Watanebe, A. 2003. Peak response prediction rule for a SDOF elasto-plastic system based on equivalent linearization technique. *Journal of Structural and Construction Engineering* (Transactions of AIJ), Vol. 68, No. 571, pp. 53-62. (in Japanese)

Kitahara, K. and Itoh, Y. 1999. A correlation between elasto-plastic dynamic response of steel and RC piers and natural period-dependent spectrum intensity. *Journal of Structural Engineering*, Vol. 45A, pp. 829-838. (in Japanese)

Kitahara, K. and Itoh, Y. 2000. Correlation between Nonlinear Response of Bridge Piers and Natural-Period-Dependent Spectrum Intensity. *Proceedings of 12 WCEE*, Paper No. 0806.

Luco, N. and Cornell, C. A. 2007. Structure-specific scalar intensity measures for near-source and ordinary earthquake ground motions. *Earthquake Spectra,* Vol. 23, pp. 357-392.

Mori, Y., Yamanaka, T., and Nakashima, M. 2004. Estimation of displacement response of steel moment frame considering post elastic-modal shape. *Journal of Structural Engineering*, AIJ, Vol. 50B, pp. 425-434. (in Japanese)

Mori, Y., Yamanaka, T., Luco, N., and Cornell, C. A. 2006. A static predictor of seismic demand on frames based on a post-elastic deflected shape. *Earthquake Engineering and Structural Dynamics*, Vol. 35, pp. 1295-1318.

Mori, Y., Mizutani, Y., and Kang, J. D. 2018. Upgrade decision-making for earthquake-vulnerable wooden houses using probabilistic damage index functions. *ASCE-ASME Journal of Risk Uncertainty Engineering Systems,* Part A: Civil Engineering, Vol. 4, No. 1, Paper No. 04017037.

Shimazaki, K. 1999. Evaluation of structural coefficient Ds by displacement response estimation using the equivalent linearization technique. *Journal of Structural and Construction Engineering* (Transactions of AIJ), Vol. 64, No. 516, pp. 51-57. (in Japanese)